**Biogeosciences
Discussions**

Does terrestrial drought explain global CO$_2$ flux anomalies induced by El Niño?

C. R. Schwalm[1], C. A. Williams[1], K. Schaefer[2], I. Baker[3], G. J. Collatz[4], and
C. Rödenbeck[5]

[1]Graduate School of Geography, Clark University, Worcester, MA 01610, USA
[2]National Snow and Ice Data Center, Cooperative Institute for Research in Environmental
Sciences, University of Colorado at Boulder, Boulder, CO 80309, USA
[3]Department of Atmospheric Science, Colorado State University, Fort Collins, CO 80523, USA
[4]Hydrospheric and Biospheric Sciences Laboratory, NASA Goddard Space Flight Center,
Greenbelt, MD 20771, USA
[5]Max Planck Institute for Biogeochemistry, 07701 Jena, Germany

Correspondence to: C. R. Schwalm (cschwalm@clarku.edu)

BGD

8, 4209–4238, 2011

**Does terrestrial
drought explain
global CO$_2$ flux
anomalies?**

C. R. Schwalm et al.

Title Page

Abstract	Introduction
Conclusions	References
Tables	Figures

◄◄   ►►

◄   ►

Back   Close

Full Screen / Esc

Printer-friendly Version

Interactive Discussion

Abstract

The El Niño Southern Oscillation is the dominant year-to-year mode of global climate variability. El Niño effects on terrestrial carbon cycling are mediated by associated climate anomalies, primarily drought, influencing fire emissions and biotic net ecosystem exchange (NEE). Here we evaluate whether El Niño produces a consistent response from the global carbon cycle. We apply a novel bottom-up approach to estimating global NEE anomalies based on FLUXNET data using land cover maps and weather reanalysis. We analyze 13 yr (1997–2009) of globally gridded observational NEE anomalies derived from eddy covariance flux data, remotely-sensed fire emissions at the monthly time step, and NEE estimated from an atmospheric transport inversion. We evaluate the overall consistency of biospheric response to El Niño and, more generally, the link between global CO$_2$ flux anomalies and El Niño-induced drought. Our findings, which are robust relative to uncertainty in both methods and time-lags in response, indicate that each event has a different spatial signature with only limited spatial coherence in Amazônia, Australia and southern Africa. For most regions, the sign of response changed across El Niño events. Biotic NEE anomalies, across 5 El Niño events, ranged from −1.34 to +0.98 Pg C yr^{-1}, whereas fire emissions anomalies were generally smaller in magnitude (ranging from −0.49 to +0.53 Pg C yr^{-1}). Overall drought does not appear to impose consistent terrestrial CO$_2$ flux anomalies during El Niños, finding large variation in globally integrated responses from −1.15 to +0.49 Pg C yr^{-1}. Contrary to previous accounts we find El Niño events have, when globally integrated, both enhanced and weakened terrestrial sink strength, with no consistent response across events.

1 Introduction

The El Niño/Southern Oscillation (ENSO), a global atmospheric circulation feature linked to atmospheric pressure patterns and sea surface temperature anomalies in

the tropical Pacific (McPhaden et al., 2006), is the dominant mode of global year-to-year climate variation (Buermann et al., 2003; Trenberth et al., 2007). Although ENSO originates in the equatorial east Pacific ocean it influences terrestrial carbon cycling globally through teleconnections to water balance (McPhaden et al., 2006; Ropelewski
5 and Halpert, 1986, 1987; Reichenau and Esser, 2003; Williams and Hanan, 2010; Woodward et al., 2008), temperature (McPhaden et al., 2006; Nagai et al., 2007), and fire emissions (Page et al., 2008; van der Werf et al., 2004, 2006).

The net effect of ENSO on terrestrial carbon cycling is assumed to be linked to its phase, with the warmer El Niño phase commonly associated with a decrease in terres-
10 trial uptake of CO_2 (Gurney et al., 2008; Jones et al., 2001; Rödenbeck et al., 2003; Qian et al., 2008). On a regional to continental scale El Niño events have been reported to have distinct spatial signatures with coherent responses, e.g., warmer and drier conditions in Tropical Asia during the dry season (Woodward et al., 2008), droughts and reduced net carbon uptake in Amazônia (Aragão et al., 2007), and enhanced fire emis-
15 sions, especially in insular Southeast Asia (van der Werf et al., 2006).

El Niño reportedly influences both the net carbon uptake by ecosystems and carbon emissions by fires, though the relative contribution of both factors remains uncertain and poorly constrained in time and space (Canadell et al., 2007b). Most studies emphasize either fire emissions (Fuller and Murphy, 2006; Langner and Siegert, 2009;
20 Page et al., 2008; Patra et al., 2005; Rödenbeck et al., 2003; van der Werf et al., 2004) or biotic NEE (Adams and Piovesan, 2005; Hasimoto et al., 2004; Reichenau et al., 2003; Woodward et al., 2008; Zeng et al., 2005). Reports documenting the biotic component have relied heavily on ecosystem process models to describe carbon cycle responses to climate fluctuations. While these explicitly incorporate biophysi-
25 cal and/or biogeochemical mechanisms they perform poorly when simulating observed NEE (Schwalm et al., 2010b).

Inversion approaches based on atmospheric CO_2 measurements have also been used to diagnose changes in carbon flux induced by El Niño events. These identify large-scale net sources/sinks and, despite substantial variation in absolute magnitude,

typically report similar interannual variability (Gurney et al., 2008). Such consistency is not surprising considering these inversions all use the same observations of atmospheric CO_2 concentration. The network of CO_2 observations is also severely underconstrained, making it difficult for inversions to resolve regional carbon fluxes, particularly in the tropics (Gurney et al., 2003).

FLUXNET offers an alternative to ecosystem process models or atmospheric inversions to evaluate the influence of El Niño events on the global carbon cycle. FLUXNET is a network of globally distributed eddy covariance towers with dense data streams of observed in situ CO_2 exchange and ancillary variables (Baldocchi, 2008). The extended spatiotemporal coverage of FLUXNET allows for the climate sensitivity of terrestrial CO_2 flux to be scaled up to estimate global flux using various data-driven approaches (Beer et al., 2010; Jung et al., 2009; Schwalm et al., 2010a; Xiao et al., 2008).

Here we investigate whether global CO_2 flux anomalies have a clear spatial signature and consistent response during El Niño events. We calculate NEE response to El Niño events from 1997–2009 using a novel upscaling approach based on micrometeorological observations of CO_2 exchange, plus fire emissions from a forward biogeochemical model and remotely-sensed estimates of area burned, fire activity, and plant productivity. Total biospheric response to El Niño events is based on monthly anomalies: NEE sensitivities to drought derived from FLUXNET (Schwalm et al., 2010a) are spatially and temporally scaled and then combined with fire emissions anomalies. We generate globally gridded monthly anomaly maps of NEE and fire emissions components of terrestrial carbon sink response. Our objective is to evaluate spatial and temporal coherence in terrestrial carbon flux response during El Niño events and to quantify the degree to which hydroclimatic anomalies during El Niño events influence the terrestrial carbon cycle.

Title Page

Abstract | Introduction

Conclusions | References

Tables | Figures

◄ | ►

◄ | ►

Back | Close

Full Screen / Esc

Printer-friendly Version

Interactive Discussion

2 Methods

Our method isolates drought-related El Niño effects on biotic NEE. We also account for fire as a carbon source as fire emissions have been shown to increase during El Niño events. We estimated these 2 components using independent sources of data and added them to quantify total biospheric response to El Niño on a monthly time step. We based the biotic NEE on scaled ecosystem sensitivities (Schwalm et al., 2010a) derived from FLUXNET data (Baldocchi, 2008). These sensitivities quantified the change in NEE for a unit change in relative water deficit anomaly where water deficit, calculated as the ratio of latent heat to available energy, represented drought (Schwalm et al., 2010a). NEE was expressed using the atmospheric convention, a positive value indicates outgassing of CO_2 to the atmosphere.

To calculate monthly ecosystem sensitivities, monthly integrals of tower-based NEE and water deficit were first normalized by month and site. That is, for each site's monthly time series, the mean monthly cycle of both NEE and water deficit were normalized by subtracting the mean and dividing by the standard deviation, which gave, in units of standard deviation, the departure from the mean value or relative anomaly (z-scores). Next, both sets of monthly relative anomalies were grouped by climatic season and site-specific land cover class according to the International Geosphere-Biosphere Program land cover classification (IGBP, Loveland et al., 2001). We then regressed the relative flux anomaly on relative water deficit anomaly within each IGBP class and climatic season. Regression in normalized space corrected for spatial gradients in the FLUXNET data compilation (Lauenroth and Sala, 1992) and yielded a linear relationship with the slope parameter representing flux sensitivity, i.e., change in relative NEE anomaly for a unit change in relative water deficit anomaly (Schwalm et al., 2010a). These dimensionless sensitivities were transformed into NEE sensitivities ($g\,C\,m^{-2}\,month^{-1}\,\sigma^{-1}$), where σ (standard deviation) referred to a 1 unit change in relative water deficit anomaly (negative values indicated increased dryness), using the standard deviation of NEE in absolute units. The NEE sensitivities were derived using

5173 months of FLUXNET data (Baldocchi, 2008) collected between 1991 and 2006 from 238 measurement towers (11 distinct land cover classes) distributed globally with the highest tower densities in North America and Europe (see Schwalm et al., 2010a for details).

Monthly NEE sensitivities to water deficit were then spatially scaled using a land cover scheme. In parallel to the IGBP designation for each flux tower, the IGBP land cover dataset includes fractional values for all possible 18 classes for the full global land surface (Loveland et al., 2001). The NEE sensitivity of each terrestrial pixel ($1° \times 1°$) was either estimated from FLUXNET (vegetated types, Schwalm et al., 2010a) or effectively 0 (non-vegetated types, e.g., urban and built up). We combined observed NEE sensitivities with fractional land cover for each pixel using a weighted sum across all IGBP class-specific sensitivities where fractional coverages served as weights. As NEE sensitivities were derived monthly by climatic season, e.g., December, January, February as winter in the northern and summer in the Southern Hemisphere, this resulted in 4 distinct sensitivity maps (Schwalm et al., 2010a), whereby the assigned sensitivities for each month within a climatic season were identical.

These pixel-specific sensitivities were subsequently temporally scaled using monthly values of water deficit from the Modern Era Retrospective-analysis for Research and Applications (MERRA, Bosilovich et al., 2008). As with FLUXNET data, water deficit was calculated as the ratio of latent heat to available energy. Each pixel was normalized by month; each month across the 1997–2009 period had a mean value of 0 and $\sigma = 1$. While MERRA data extends from 1979–present the 1997–2009 period was chosen to match the temporal coverage of fire emissions data (see below). The normalization resulted in a monthly grid of water deficit relative anomalies for all 156 months in the 13-yr record. These grids were combined with the climatic season-specific grids of NEE sensitivity to generate spatial fields of flux anomaly for each month:

$$\Delta_{biotic} = \frac{d\text{NEE}}{dz} z, \tag{1}$$

Full Screen / Esc

Printer-friendly Version

Interactive Discussion

where, for any given month and pixel, Δ_{biotic} ($g\,C\,m^{-2}\,month^{-1}$) is the NEE flux anomaly, $d\mathrm{NEE}/dz$ is the pixel- and climatic season-specific NEE sensitivity to water deficit ($g\,C\,m^{-2}\,month^{-1}\,\sigma^{-1}$), and z is the monthly pixel-specific relative anomaly of water deficit in σ units.

5   The principal strength of this approach is its reliance on observations of in situ CO_2 exchange as it responds to a single driver, water deficit. The derived sensitivities isolate hydroclimatic effects while excluding potentially confounding covariates. This allows a conditional analysis of the carbon consequences of El Niño predicated on a robust relationship with drought. Alternatively, El Niño is analyzed as a drought phenomenon

10   based on its large influence on water balance in general and precipitation in particular (e.g., Ropelewski and Halpert, 1986, 1987; Williams and Hanan, 2010). Previous diagnostic attempts to upscale point-based eddy covariance data, i.e., to move from site-specific anecdotes to spatially explicit large-scale characterizations, have typically featured data mining algorithms (Beer et al., 2010; Jung et al., 2008, 2009; Papale and

15   Valentini, 2003; Vetter et al., 2008; Xiao et al., 2008; Yang et al., 2006, 2007). While such approaches may show high skill in matching observed or reference fields, as black-box algorithms they provide less insight into the underlying mechanisms, drought in this case. Our technique enables a direct examination of the El Niño effects on terrestrial carbon cycling.

20   The second component of total biospheric response, fire emissions anomalies (Δ_{fire}, $g\,C\,m^{-2}\,month^{-1}$), was derived from monthly data in the Global Fire Emissions Database (GFED) version 3.1 (Randerson et al., 2007; van der Werf et al., 2006, 2010). For each grid cell the mean monthly seasonal cycle from 1997–2009 was removed with the remainder giving Δ_{fire}. Both fire and biotic anomalies shared the same spatial res-

25   olution ($1° \times 1°$) and were added to estimate the total drought-related terrestrial carbon sink response (Δ_{total}) by pixel to an El Niño event. All anomalies (Δ_{biotic}, Δ_{fire}, and Δ_{total}) represent the monthly deviation from the mean monthly cycle across the full analysis period from 1997–2009 where positive anomalies indicate increased CO_2 outgassing to the atmosphere relative to the 13-yr mean.

El Niño events were determined using the Multivariate ENSO Index (MEI, Wolter and Timlin, 1998). The bimonthly MEI values were indexed by their last month, e.g., December–January was indexed as January. Any given month was classified as an El Niño condition if its bimonthly MEI value lay in the upper tercile of all bimonthly MEI values from December 1949–January 1950 through November–December 2009. El Niño events of 3 months or less were discarded. Internal gaps (MEI values outside the upper tercile) of 1 month were still counted as the same event. For each El Niño event, the terrestrial carbon sink anomaly for each pixel was summed across all its months. Global event totals were estimated by aggregating over the full terrestrial land surface.

Fire emissions and biotic NEE response to El Niño may, with considerable across-study variability, exhibit a lagged response (e.g., Fuller and Murphy, 2006; Qian et al., 2008; Wooster et al., 2011). We analyzed the effect of a potentially delayed response of carbon cycling to El Niño by estimating lags (l_{MEI}) between MEI and flux anomalies using the highest (in absolute value) statistically significant cross-correlation and by calculating lagged correlations as well as global event totals using time-lags (flux response lags MEI) of up to 6 months.

We estimated uncertainty for Δ_{biotic}, Δ_{fire}, and Δ_{total} as one standard deviation about the mean value (1σ). For Δ_{biotic}, 2 sources of uncertainty were considered: uncertainty in NEE sensitivity and uncertainty in MERRA reanalysis field. The latter was based on the dispersion of multiple overlapping retrospective analyses. We used the Multi-model Analysis for the Coordinated Enhanced Observing Period dataset (CEOP, Bosilovich et al., 2009), an ensemble of 10 global reanalysis products, including MERRA, from October 2002–December 2004 (ftp://agdisc.gsfc.nasa.gov/private/ceop/), and calculated 1σ across all ensemble members for each terrestrial pixel. These values were then averaged by month to create a mean annual cycle of monthly uncertainty used for the full hindcast period. For the relation between NEE and water deficit, i.e., NEE sensitivity, we used the uncertainty associated with the slope parameter from standard regression techniques (Cook and Weisberg, 1999). This method provided the mean (the value used in the reported NEE anomalies) and 1σ for both sources which were

then combined using Monte Carlo methods as follows: (i) for all pixels and all months randomly draw from a Gaussian distribution a realization of NEE sensitivity ($d\text{NEE}/dz$; Eq. 1) and water deficit. (ii) Normalize water deficit to generate z (Eq. 1). (iii) Calculate Δ_{biotic} for all pixels and all months. (iv) Repeat this process 1000 times. This generated 1000 realizations of the 156 month analysis period with uncertainty of $\Delta_{\text{biotic}}(= \varepsilon_{\text{biotic}})$ given by 1σ across the full set.

For Δ_{fire} only yearly uncertainties are available. We used a 20% relative error for globally integrated annual integrals: $\varepsilon_{\text{fire}} = 0.20\,\Delta_{\text{fire}}$ (van der Werf et al., 2010). Uncertainty for the total flux anomaly, for annual values only, combined both components in quadrature: $\varepsilon_{\text{total}} = \sqrt{\varepsilon_{\text{fire}}^2 + \varepsilon_{\text{biotic}}^2}$. Furthermore, we created a map of $\varepsilon_{\text{biotic}}$ and its component sources of error using a weighted average across all months with weights based on monthly f_{APAR} (fraction of photosynthetically active radiation absorbed by vegetation) normals, an independent measure of seasonal variability in vegetation productivity. Monthly normals of f_{APAR} were derived from the Global Inventory Monitoring and Modeling Study (GIMMS; Tucker et al., 2005).

Lastly, we compared our bottom-up flux anomalies with top-down estimates from the 1997–2008 Jena CO_2 inversion (3.75° × 5°; run s96_v3.2; update of Rödenbeck et al., 2003, 2005; http://www.bgc-jena.mpg.de/~christian.roedenbeck/download-CO2/). These were based on CO_2 concentrations translated into flux anomalies with a global atmospheric tracer transport model. From the inversion estimates, only the globally integrated terrestrial flux was considered (fossil fuel emissions and ocean exchange were excluded). Anomalies were estimated similar to GFED data: the mean monthly seasonal cycle from 1997–2008 was removed with the remainder giving the total NEE anomaly. Uncertainty was quantified as the mean absolute deviation across an ensemble of 6 runs (update of Rödenbeck et al., 2003, 2005) aggregated to annualized event totals.

3   Results and discussion

The sign of Δ_{biotic} across all 5 El Niño events showed spatial coherence in several regions (Fig. 1a): $\Delta_{biotic} > 0$ occurred primarily in Australasia, southern Africa, and parts of Amazônia. In contrast, regions where the terrestrial carbon sink was enhanced ($\Delta_{biotic} < 0$) were located in the continental United States (excluding the Upper Great Plains), tropical Africa, northern and southern South America as well as more stippled patterns throughout Eurasia. Patterns for the sign of Δ_{fire} (not shown) were more diffuse (both signs intermixed without a clear emergent spatial reference) with loose clusters of positive pixels in Indonesia, Japan, and northern South America as well as negative pixels (less fire emissions than the long-term average) across much of the Northern Hemisphere.

These coherently signed anomalies for both Δ_{biotic} and Δ_{fire} were however small in magnitude and occurred on less than ~3 % of the vegetated land surface. The 5 El Niño events observed with GFED and scaled FLUXNET sensitivities consisted of 55 months, excluding internal gap months. Using a false discovery rate of 0.05 (Ventura et al., 2004) with all El Niño months as replicates revealed 407 Δ_{fire} pixels (of a possible 12371 vegetated pixels) with non-zero mean values and only 4 with $|\Delta_{fire}| > 10\,\mathrm{g\,C\,m^{-2}\,month^{-1}}$. For Δ_{biotic} only 5 grid cells showed a non-zero mean (largest magnitude $= -2.1\,\mathrm{g\,C\,m^{-2}\,month^{-1}}$) across all El Niño months.

The magnitude of non-zero anomalies coupled with their scarcity is strong evidence that the responses across El Niño events were inconsistent and not statistically robust in time or space. This is further supported by Jena inversion results (Fig. 1b). These implicitly comprise fire emissions and biotic components and also showed minimal across-event consistency in carbon sink sign anomaly. Similarly, globally aggregated El Niño anomalies from 1997–2009 (Table 1) were highly variable. This ambiguity of El Niño as a control on CO_2 sources/sinks was also present in event-based derivative totals, i.e., the time derivative of Δ_{biotic} during each event showed inconsistent sign and no relationship with sign of total Δ_{biotic} anomaly by event (not shown). While Δ_{fire} was generally positive (enhanced outgassing of CO_2 to the atmosphere), Δ_{biotic} was negative

for 2 of 5 events with Δ_{total} ranging from -1.15 to $+0.49\,Pg\,C\,yr^{-1}$ relative to the 2000–2006 average sink of $-2.8\,Pg\,C\,yr^{-1}$ (Canadell et al., 2007a). Inversion-constrained estimates showed more variability and ranged from -1.01 to $+2.48\,Pg\,C\,yr^{-1}$.

Event-based flux anomaly totals adjusted for potential lags also showed no consistent response across El Niño events. Across a range of lags (l_{MEI}) from 0 to 6 months, globally aggregated El Niño flux anomalies displayed no coherent response (Fig. 2). Whereas Δ_{biotic} (Fig. 2a) showed the most variability in event-based totals, Δ_{fire} at lags of 4 months or more (Fig. 2b) was always positive. El Niño acted to both increase and decrease terrestrial carbon sink strength at all lags across the 5 observed events.

Each El Niño event was largely unique in its spatial signature. Some grid cell clusters of Δ_{biotic} consistent response (Fig. 3) were present across at least 3 events and corresponded to well-established zones of influence: the dipole pattern in sub-Saharan Africa as well as the juxtaposition of regions with CO_2 loss and uptake in South America. Other regions of biotic response have not been previously documented: an east-west swath from Central Siberia to the Iberian Peninsula showed numerous pixels with $|\Delta_{biotic}| > 50\,g\,C\,m^{-2}\,yr^{-1}$ but of variable sign. Lastly, India and Indonesia, generally assumed to be drier during El Niño events, were also variable in sign. For Δ_{fire} (Fig. 4) patterns were more consistent albeit sparser. The same regions showed a response in all events, especially Indonesia, with changes in sign apparent in the northern high latitudes.

Variability across these 5 El Niño events was large, in contrast to previous studies (Gurney et al., 2008; Jones et al., 2001; Rödenbeck et al., 2003; Qian et al., 2008), and most regions showed responses that switched sign across events (cf. Bousquet et al., 2000). This was largely confined to the biotic component. On a globally integrated basis Δ_{fire} shifted from -0.13 to $+0.16\,Pg\,C\,month^{-1}$ during normal conditions to -0.09 to $+0.19\,Pg\,C\,month^{-1}$ across all El Niño months. This highlighted a general tendency of increased fire emissions during El Niño events (Table 1). The same tendency was not evident for Δ_{biotic}, which exhibited more variability outside El Niño events than during: -0.35 to $+0.38$ vs. -0.29 to $+0.33\,Pg\,C\,month^{-1}$, respectively.

Does terrestrial drought explain global CO$_2$ flux anomalies?

C. R. Schwalm et al.

This lack of consistent response in space or time occurred despite a significant correlation between MEI and monthly terrestrial carbon sink anomalies (Fig. 5) across the full 13-yr data record (cf. Patra et al., 2005). This was the case for both the Jena inversion ($r = 0.41$, $p < 0.001$) and Δ_{fire} ($r = 0.30$, $p < 0.001$). No significant correlation was found using either biotic or total flux anomaly from the bottom-up method. Allowing for a lagged response ($l_{\text{MEI}} = $ lag with maximal correlation) altered these values for the Jena inversion ($l_{\text{MEI}} = 3$, $r = 0.51$, $p < 0.05$), Δ_{fire} ($l_{\text{MEI}} = 4$, $r = 0.47$, $p < 0.05$), and Δ_{biotic} ($l_{\text{MEI}} = 6$, $r = 0.25$, $p < 0.05$). No change, and no significant lag, was found for Δ_{total}.

In the spatial domain MEI and water deficit exhibited a clear teleconnection. Large-scale teleconnective clusters with similar signed correlation occurred globally but were sparser in Russia (Fig. 6a). Similarly, Jena inversion results and Δ_{total} (Fig. 6b and c) showed significant correlations with MEI. While both flux responses exhibited similarities in the aggregate, the larger grid cell ($3.75° \times 5°$) of the Jena results masked smaller-scaled features in several regions, e.g., the dipole pattern in sub-Saharan Africa. Comparing lagged to unlagged teleconnection maps (not shown), the highest correlation, in absolute value, increased from 0.59 (cf. Fig. 6b) to 0.61 and the median value increased from 0.39 to 0.41.

Overall, the temporal correlation and spatial teleconnection were not sufficient to regularize terrestrial carbon sink response to El Niño. While correlations were significant for both the top-down and bottom-up methods and approached 0.6 in magnitude (Fig. 6b), this only equated to ~36 % variation explained in the best case. The amount of variation explained by El Niño was also constrained by the 13-yr analysis period. This length effectively precluded elimination of longer-term and possibly confounding trends or cyclical phenomena such as changes in soil moisture limitation (Jung et al., 2010), global dimming and brightening (Wild, 2009), and El Niño type based on spatial signatures of equatorward sea surface temperature anomalies (Collins et al., 2010; Yeh et al., 2009). Thus, ENSO as a mode of global climate variability (with or without a time-lag response) cannot constrain terrestrial sink behaviour as the majority of

variation remained unaccounted for. As a result the terrestrial integrated signal of the 5 observed El Niño events was not consistent.

These observed dynamics were present even within the context of uncertainty. Spatial patterns in $\varepsilon_{\text{biotic}}$ showed more similarity to uncertainties in NEE sensitivity as opposed to reanalyzed water deficit (Fig. 7). Monthly values of $\varepsilon_{\text{biotic}}$ were highly left-skewed with a mean of $6.5\,\text{g C m}^{-2}\,\text{month}^{-1}$ and a maximum value of $43.1\,\text{g C m}^{-2}\,\text{month}^{-1}$, co-located in a cluster of relatively high values in Manitoba, Canada. Higher values of $\varepsilon_{\text{biotic}}$ generally occurred in areas dominated by croplands including the Great Plains region of North America, central Russia, and China (Fig. 7c).

Uncertainty values decreased when aggregated to longer time scales and larger spatial domains. Average yearly $\varepsilon_{\text{biotic}}$ by pixel, based on summation in quadrature, was $22.5\,\text{g C m}^{-2}\,\text{yr}^{-1}$. Furthermore, integrated globally and aggregated to annualized El Niño events, uncertainty was generally an order of magnitude less than flux anomaly (Table 1) and ranged from 4 % (2006/2007 event) to 40 % (1997/1998 event). In all cases, 95 % confidence intervals did not include 0, i.e., all Δ_{biotic}, Δ_{fire}, and Δ_{total} single event totals were statistically non-zero.

Both the tower upscaling and atmospheric inversion approaches exhibited large across-event variability in the spatial pattern and magnitude of carbon flux responses to El Niño. However, there was no overlap between the 2 estimates of total annualized anomaly; Rödenbeck et al. (2003) anomalies were outside 95 % confidence bounds of the bottom-up Δ_{total} for all events (Table 1). Spatially, large-scale regions of agreement (Fig. 1) were found only in southern Africa and northern Europe. This general lack of correspondence between bottom-up and top-down approaches derives from underlying methodological limitations and assumptions:

1. The top-down method quantifies total surface-atmosphere CO$_2$ exchange, while the upscaling method was constrained to solely address El Niño-induced drought effects using water deficit and changes in fire emissions. Thus, the top-down inversion includes other factors, e.g., possible light and temperature drivers of El Niño-induced anomalies in CO$_2$ exchange, as well as any longer-term trends

associated with global environmental change such as a general increase in temperatures (Meehl et al., 2007; Trenberth et al., 2007) and CO_2 fertilization (Friedlingstein et al., 2006).

2. The CO_2 concentrations and flux tower networks both drastically undersample the tropics (sensu Scholes et al., 2009). This is problematic insomuch as the impact of El Niño events on the terrestrial biosphere is assumed larger in the tropics than elsewhere (McPhaden et al., 2006). Although the tropical region is undersampled in both networks, the FLUXNET-based bottom-up approach achieves a relatively high degree of representativeness for this region (cf. Sundareshwar et al., 2007). In contrast, undersampling in the tropics makes it difficult for inversions to resolve fluxes in tropical Africa vs. tropical South America (Gurney et al., 2003).

3. Different input datasets introduce uncertainty in both methods. MERRA is a re-analyzed product. While ∼4 million observations are assimilated each 6-h period (http://gmao.gsfc.nasa.gov/merra/) the gridded reanalyzed fields were ultimately generated using a land surface model (LSM). For MERRA the Catchment LSM (Koster et al., 2000), embedded in the Goddard Earth Observing System Model, Version 5 (GEOS-5), was used. Although Catchment LSM has been shown to perform well in model evaluation examinations (e.g., Dirmeyer et al., 2006) model errors could still propagate through the bottom-up approach. For the Jena inversion results uncertainty was in the transport model and meteorological forcing data. Thus, we quantified the uncertainty associated with reanalyzed water deficit and propagated this through to flux anomalies and showed that our findings were robust after discounting this uncertainty as well as the uncertainty associated with the Jena results (Table 1).

4. Sub-grid variability for the Jena product was larger than for the bottom-up approach based on their respective resolutions: $3.75° × 5°$ for Jena and $1° × 1°$ for the bottom-up approach. More important than the pixel size is the larger a priori correlation length which forced the inversion to be smooth on at least a 1200 km

Does terrestrial drought explain global CO_2 flux anomalies?

C. R. Schwalm et al.

scale (Rödenbeck et al., 2003). This, coupled with known issues of spatial resolution in inversion-constrained estimates (e.g., Gurney et al., 2003), biased the spatial intercomparisons.

Our results clearly show that El Niño events do not produce a consistent CO$_2$ response from the terrestrial biosphere, even though top-down and bottom-up estimates did not show statistical agreement in response. High variability in total biospheric anomaly, both across-method and within-method, underscored the general lack of consistent pattern of terrestrial sink response to El Niño. In addition, both bottom-up and top-down methods revealed that El Niño does not impose a coherent across-event response regarding the integrated global terrestrial response as well as its spatial patterning. Finally, even though monthly time series of global net terrestrial-atmosphere CO$_2$ flux anomalies were significantly correlated with MEI for both approaches (flux upscaled and atmospheric inversion), this did not result in the canonical expectation of increased CO$_2$ outgassing during El Niño events.

4 Conclusions

There is no consistent response of terrestrial carbon cycling to El Niño events. The significant correlation between MEI and global CO$_2$ flux anomalies, estimated using either approach, did not translate into spatiotemporal consistency in terrestrial sink response to El Niño. Although we cannot exclude confounding longer-term trends or periodicities based on the time domain of this analysis, our results indicate that drought is insufficient to constrain the effects of El Niño on carbon cycling. While ENSO is the dominant mode of year-to-year climatic variability, this was not reflected in global CO$_2$ flux anomalies. Importantly, the bottom-up, data-oriented approach presented here indicates that El Niño events may act to either enhance or diminish terrestrial carbon uptake. This is in contrast to the prevailing view that El Niño induces CO$_2$ releases by stimulating drought. Furthermore all 5 El Niño events across the 13-yr

record displayed a unique Δ_{biotic} spatial signature with only limited coherence in parts of Amazônia, Australia and southern Africa. Across all events, fire emissions anomalies were smaller in magnitude than biotic anomalies of CO_2 exchange except during the 1997/1998 El Niño event, i.e., the global terrestrial response to El Niño is driven more by the biotic component than by fire. Lastly, the bottom-up scaling approach detailed here is a biologically interpretable and efficient method to extend the kernel of observed FLUXNET data to large-scale spatially explicit patterns of carbon cycle dynamics.

References

Adams, J. M. and Piovesan, G.: Long series relationships between global interannual CO_2 increment and climate: Evidence for stability and change in role of the tropical and boreal-temperate zones, Chemosphere, 59, 1595–1612, 2005.

Aragão, L., Malhi, Y., Roman-Cuesta, R. M., Saatchi, S., Anderson, L. O., and Shimabukuro, Y. E.: Spatial patterns and fire response of recent Amazonian droughts, Geophys. Res. Lett., 34(5), L07701, doi:10.1029/2006GL028946, 2007.

Baldocchi, D.: Breathing of the terrestrial biosphere: lessons learned from a global network of carbon dioxide flux measurement systems, Aust. J. Bot., 56, 1–26, 2008.

Beer, C., Reichstein, M., Tomelleri, E., Ciais, P., Jung, M., Carvalhais, N., Rödenbeck, C., Arain, M. A., Baldocchi, D., Bonan, G. B., Bondeau, A., Cescatti, A., Lasslop, G., Lindroth, A., Lomas, M., Luyssaert, S., Margolis, H., Oleson, K. W., Roupsard, O., Veenendaal, E., Viovy, N., Williams, C., Woodward, F. I., and Papale, D.: Terrestrial gross carbon dioxide uptake: Global distribution and covariation with climate, Science, 329, 834–838, 2010.

Bosilovich, M., Chen, J., Robertson, F. R., and Adler, R. F.: Evaluation of global precipitation in reanalyses, J. Appl. Meteorol. Clim., 47, 2279–2299, 2008.

Bosilovich, M., Mocko, D., Roads, J. O., and Ruane, A.: A multimodal analysis for

the Coordinated Enhanced Observing Period (CEOP), J. Hydrometeorol., 10, 912–934, doi:10.1175/2009JHM1090.1, 2009.

Bousquet, P., Peylin, P., Ciais, P., Quéré, C. L., Friedlingstein, P., and Tans, P. P.: Regional changes in carbon dioxide fluxes of land and oceans since 1980, Science, 290, 1342–1346, 2000.

Brönnimann, S., Xoplaki, E., Casty, C., Pauling, A., and Luterbacher, J.: ENSO influence on Europe during the last centuries, Clim. Dynam., 28, 181–197, doi:10.1007/s00382-006-0175-z, 2007.

Buermann, W., Anderson, B., Tucker, C. J., Dickinson, R. E., Lucht, W., Potter, C. S., and Myneni, R. B.: Interannual covariability in Northern Hemisphere air temperatures and greenness associated with El Niño-Southern Oscillation and the Arctic oscillation, J. Geophys. Res., 108(D13), 4396, doi:10.1029/2002JD002630, 2003.

Canadell, J. G., Le Quéré, C., Raupach, M. R., Field, C. B., Buitenhuis, E. T., Ciais, P., Conway, T. J., Gillett, N. P., Houghton, R. A., and Marland, G.: Contributions to accelerating atmospheric CO$_2$ growth from economic activity, carbon intensity, and efficiency of natural sinks, Proc. Natl. Acad. Sci., 104, 18866–18870, 2007a.

Canadell, J. G., Pataki, D. E., Gifford, R., Houghton, R. A., Luo, Y., Raupach, M. R., Smith, P., and Steffen, W.: Saturation of the terrestrial carbon sink, in: Terrestrial Ecosystems in a Changing World. The IGBP Series, edited by: Canadell, J. G., Pataki, D., and Pitelka, L., Springer-Verlag, Berlin, 59–73, 2007b.

Collins, M., An, S.-I., Cai, W., Ganachaud, A., Guilyardi, E., Jin, F.-F., Jochum, M., Lengaigne, M., Power, S., Timmermann, A., Vecchi, G., and Wittenberg, A.: The impact of global warming on the tropical Pacific Ocean and El Niño, Nat. Geosci., 3, 391–397, 2010.

Cook, R. D. and Weisberg, S.: Applied Regression Including Computing and Graphics, Wiley-Interscience, New York, NY, 632 pp., 1999.

Dirmeyer, P. A., Gao, X., Zhao, M., Guo, Z.-C., Oki, T., and Hanasaki, N.: The Second Global Soil Wetness Project (GSWP-2): Multi-model analysis and implications for our perception of the land surface, B. Am. Meteorol. Soc., 87, 1381–1397, 2006.

Fuller, D. O. and Murphy, K.: The ENSO-fire dynamic in insular Southeast Asia, Climatic Change, 74, 435–455, 2006.

Friedlingstein, P., Cox, P., Betts, R., Bopp, L., Von Bloh, W., Brovkin, V., Cadule, P., Doney, S., Eby, M., Fung, I., Bala, G., John, J., Jones, C., Joos, F., Kato, T., Kawamiya, M., Knorr, W., Lindsay, K., Matthews, H. D., Raddatz, T., Rayner, P., Reick, C., Roeckner, E., Schnitzler, K.

G., Schnur, R., Strassmann, K., Weaver, A. J., Yoshikawa, C., and Zeng, N.: Climate-carbon cycle feedback analysis: Results from the (CMIP)-M-4 model intercomparison, J. Climate, 19(14), 3337–3353, 2006.

Gurney, K. R., Law, R. M., Denning, A. S., Rayner, P. J., Baker, D., Bousquet, P., Bruhwiler, L., Chen, Y.-H., Ciais, P., Fan, S., Fung, I. Y., Gloor, M., Heimann, M., Higuchi, K., John, J., Kowalczyk, E., Maki, T., Maksyutov, S., Peylin, P., Prather, M., Pak, B. C., Sarmiento, J., Taguchi, S., Takahashi, T. and Yuen, C.-W.: TransCom 3 CO_2 inversion intercomparison: 1. Annual mean control results and sensitivity to transport and prior flux information, Tellus B, 55, 555–579, doi:10.1034/j.1600-0889.2003.00049.x, 2003.

Gurney, K. R., Baker, D., Rayner, P., and Denning, S.: Interannual variations in continental-scale net carbon exchange and sensitivity to observing networks estimated from atmospheric CO_2 inversions for the period 1980 to 2005, Global Biogeochem. Cy., 22, GB3025, doi:10.1029/2007GB003082, 2008.

Jones, C. D., Collins, M., Cox, P. M., and Spall, S. A.: The carbon cycle response to ENSO: A coupled climate-carbon cycle model study, J. Climate, 14, 4113–4129, 2001.

Jung, M., Verstraete, M., Gobron, N., Reichstein, M., Papale, D., Bondeau, A., Robustelli, M., and Pinty, B.: Diagnostic assessment of European gross primary production, Glob. Change Biol., 14, 2349–2364, doi:10.1111/j.1365-2486.2008.01647.x, 2008.

Jung, M., Reichstein, M., and Bondeau, A.: Towards global empirical upscaling of FLUXNET eddy covariance observations: validation of a model tree ensemble approach using a biosphere model, Biogeosciences, 6, 2001–2013, doi:10.5194/bg-6-2001-2009, 2009.

Jung, M., Reichstein, M., and Ciais, P., Seneviratne, S. I., Sheffield, J., Goulden, M. L., Bonan, G., Cescatti, A., Chen, J., de Jeu, R., Dolman, A. J., Eugster, W., Gerten, D., Gianelle, D., Gobron, N., Heinke, J., Kimball, J., Law, B. E., Montagnani, L., Mu, Q., Mueller, B., Oleson, K., Papale, D., Richardson, A. D., Roupsard, O., Running, S., Tomelleri, E., Viovy, N., Weber, U., Williams, C., Wood, E., Zaehle, S., and Zhang, K.: A recent decline in the global land evapotranspiration trend due to limited moisture supply, Nature, 467, 951–954, doi:10.1038/nature09396, 2010.

Koster, R. D., Suarez, M. J., Ducharne, A., Stieglitz, M., and Kumar, P.: A catchment-based approach to modeling land surface processes in a GCM, Part 1, Model Structure, J. Geophys. Res., 105, 24809–24822, 2000.

Langner, A. and Siegert, F.: Spatiotemporal fire occurrence in Borneo over a period of 10 years, Glob. Change Biol., 15, 48–62, 2009.

Does terrestrial drought explain global CO_2 flux anomalies?

C. R. Schwalm et al.

Lauenroth, W. K. and Sala, O. E.: Long-term forage production of North American shortgrass steppe, Ecol. Appl., 4, 397–403, 1992.

Le Page, Y., Pereira, J. M. C., Trigo, R., da Camara, C., Oom, D., and Mota, B.: Global fire activity patterns (1996–2006) and climatic influence: an analysis using the World Fire Atlas, Atmos. Chem. Phys., 8, 1911–1924, doi:10.5194/acp-8-1911-2008, 2008.

Loveland, T. R., Reed, B. C., Brown, J. F., Ohlen, D. O., Zhu, J., Yang, L., and Merchant, J. W.: Development of a global land cover characteristics database and IGBP DISCover from 1-km AVHRR data, Int. J. Remote Sens., 21, 1303–1330, 2001.

McPhaden, M. J., Zebiak, S. E., and Glantz, M. H.: ENSO as an integrating concept in the earth sciences, Science, 314, 1740–1745, 2006.

Meehl, G. A., Stocker, T. F., Collins, W. D., Friedlingstein, P., Gaye, A. T., Gregory, J. M., Kitoh, A., Knutti, R., Murphy, J. M., Noda, A., Raper, S. C. B., Watterson, I. G., Weaver, A. J., and Zhao, Z.-C.: Global Climate Projections, in: Climate Change 2007: The Physical Science Basis. Contribution of Working Group I to the Fourth Assessment Report of the Intergovernmental Panel on Climate Change, edited by: Solomon, S., Qin, D., Manning, M., Chen, Z., Marquis, M., Averyt, K. B., Tignor, M., and Miller, H. L., Cambridge University Press, Cambridge, United Kingdom and New York, NY, USA, 2007.

Nagai, S., Ichii, K., and Morimoto, H.: Interannual variations in vegetation activities and climate variability caused by ENSO in tropical rainforests, Int. J. Remote Sens., 28, 1285–1297, 2007.

Papale, D. and Valentini, A.: A new assessment of European forests carbon exchanges by eddy fluxes and artificial neural network spatialization, Glob. Change Biol., 9, 525–535, 2003.

Patra, P. K., Ishizawa, M., Maksyutov, S., Nakazawa, T., and Inoue, G.: Role of biomass burning and climate anomalies for land-atmosphere carbon fluxes based on inverse modeling of atmospheric CO_2, Global Biogeochem. Cy., 19, GB3005, doi:10.1029/2004GB002258, 2005.

Qian, H., Joseph, R., and Zeng, N.: Response of the terrestrial carbon cycle to the El Niño-Southern Oscillation, Tellus B, 60, 537–550, doi:10.1111/j.1600-0889.2008.00360.x, 2008.

Randerson, J. T., van der Werf, G. R., Giglio, L., Collatz, G. J., and Kasibhatla, P. S.: Global Fire Emissions Database, Version 3.1 (GFEDv3.1). Data set, available at: http://daac.ornl.gov/ from Oak Ridge National Laboratory Distributed Active Archive Center, Oak Ridge, Tennessee, USA, 2010.

Ropelewski, C. F. and Halpert, M. S.: North American precipitation and temperature patterns

associated with the El Niño-Southern Oscillation (ENSO), Mon. Weather Rev., 114, 2352–2362, 1986.

Ropelewski, C. F. and Halpert, M. S.: Global and regional scale precipitation patterns associated with the El Niño-Southern Oscillation, Mon. Weather Rev., 115, 1606–1626, 1987.

5 Reichenau, T. G. and Esser, G.: Is interannual fluctuation of atmospheric CO_2 dominated by combined effects of ENSO and volcanic aerosols?, Global Biogeochem. Cy., 17(4), 1094, doi:10.1029/2002GB002025, 2003.

Rödenbeck, C.: Estimating CO_2 sources and sinks from atmospheric mixing ratio measurements using a global inversion of atmospheric transport, Technical Report 6, Max

10 Planck Institute for Biogeochemistry, Jena, available at: http://www.bgc-jena.mpg.de/mpg/websiteBiogeochemie/Publikationen/Technical_Reports/tech_report6.pdf, 2005.

Rödenbeck, C., Houweling, S., Gloor, M., and Heimann, M.: CO_2 flux history 1982–2001 inferred from atmospheric data using a global inversion of atmospheric transport, Atmos. Chem. Phys., 3, 1919–1964, doi:10.5194/acp-3-1919-2003, 2003.

15 Scholes, R. J., Monteiro, P. M. S., Sabine, C. L., and Canadell, J. G.: Systematic long-term observations of the global carbon cycle, Trends Ecol. Evol., 24, 427–430, 2009.

Schwalm, C. R., Williams, C. A., Schaefer, K., Arneth, A., Bonal, D., Buchmann, N., Chen, J., Law, B. E., Lindroth, A., Luyssaert, S., Reichstein, M., and Richardson, A. D.: Assimilation exceeds respiration sensitivity to drought: A FLUXNET synthesis, Glob. Change Biol., 16,

20 657–670, doi:10.1111/j.1365-2486.2009.01991.x, 2010a.

Schwalm, C. R., Williams, C. A., Schaefer, K., Anderson, R., Arain, M. A., Baker, I., Barr, A., Black, T. A., Chen, G., Chen, J. M., Ciais, P., Davis, K. J., Desai, A., Dietze, M., Dragoni, D., Fischer, M. L., Flanagan, L. B., Grant, R., Gu, L., Hollinger, D., Izaurralde, R. C., Kucharik, C., Lafleur, P., Law, B. E., Li, L., Li, Z., Liu, S., Lokupitiya, E., Luo, Y., Ma, S., Margolis, H.,

25 Matamala, R., McCaughey, H., Monson, R. K., Oechel, W. C., Peng, C., Poulter, B., Price, D. T., Riciutto, D. M., Riley, W., Sahoo, A. K., Sprintsin, M., Sun, J., Tian, H., Tonitto, C., Verbeeck, H., and Verma, S. B.: A model-data intercomparison of CO_2 exchange across North America: Results from the North American Carbon Program site synthesis, J. Geophys. Res., 115, G00H05, doi:10.1029/2009JG001229, 2010b.

30 Sundareshwar, P. V., Murtugudde, R., Srinivasan, Singh, G. S., Ramesh, K. J., Ramesh, R., Verma, S. B., Agarwal, D., Baldocchi, D., Baru, C. K., Baruah, K. K., Chowdhury, G. R., Dadhwal, V. K., Dutt, C. B. S., Fuentes, J., Gupta, P. K., Hargrove, W. W., Howard, M., Jha, C. S., Lal, S., Michener, W. K., Mitra, A. P., Morris, J. T., Myneni, R. R., Naja, M., Nemani, R.,

Does terrestrial drought explain global CO_2 flux anomalies?

C. R. Schwalm et al.

Title Page

Abstract | Introduction

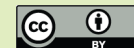Conclusions | References

Tables | Figures

◄ | ►

Back | Close

Full Screen / Esc

Printer-friendly Version

Interactive Discussion

Purvaja, R., Raha, S.,Santhana Vanan, S. K., Sharma, M., Subramaniam, A., Sukumar, R., Twilley, R. R., and Zimmerman, P. R.: Environmental monitoring network for India, Science, 316, 204–205, 2007.

Trenberth, K. E., Jones, P. D., Ambenje, P., Bojariu, R., Easterling, D., Klein Tank, A., Parker, D., Rahimzadeh, F., Renwick, J. A., Rusticucci, M., Soden, B., and Zhai, P.: Observations: Surface and Atmospheric Climate Change, in: Climate Change 2007: The Physical Science Basis. Contribution of Working Group I to the Fourth Assessment Report of the Intergovernmental Panel on Climate Change, edited by: Solomon, S., Qin, D., Manning, M., Chen, Z., Marquis, M., Averyt, K. B., Tignor, M., and Miller, H. L., Cambridge University Press, Cambridge, United Kingdom and New York, NY, USA, 2007.

Tucker, C. J., Pinzon, J. E., Brown, M. E., Slayback, D. A., Pak, E. E., Mahoney, R., Vermote E. F., and El Saleous, N.: An extended AVHRR 8-km NDVI dataset compatible with MODIS and SPOT vegetation NDVI data, Int. J. Remote Sens., 26, 4485–5598, 2005.

van der Werf, G. R., Randerson, J. T., Collatz, G. J., Giglio, L., Kasibhatla, P. S., Arellano Jr., A. F., Olsen, S. C., and Kasischke, E. S.: Continental-scale partitioning of fire emissions during the 1997 to 2001 El Nino/La Nina period, Science, 303, 73–76, 2004.

van der Werf, G. R., Randerson, J. T., Giglio, L., Collatz, G. J., Kasibhatla, P. S., and Arellano Jr., A. F.: Interannual variability in global biomass burning emissions from 1997 to 2004, Atmos. Chem. Phys., 6, 3423–3441, doi:10.5194/acp-6-3423-2006, 2006.

Ventura, V., Paciorek, C. J., and Risbey, J. S.: Controlling the proportion of falsely-rejected hypotheses when conducting multiple tests with climatological data, J. Climate, 17, 4343–4356, 2004.

Vetter, M., Churkina, G., Jung, M., Reichstein, M., Zaehle, S., Bondeau, A., Chen, Y., Ciais, P., Feser, F., Freibauer, A., Geyer, R., Jones, C., Papale, D., Tenhunen, J., Tomelleri, E., Trusilova, K., Viovy, N., and Heimann, M.: Analyzing the causes and spatial pattern of the European 2003 carbon flux anomaly using seven models, Biogeosciences, 5, 561–583, doi:10.5194/bg-5-561-2008, 2008.

Wild, M.: Global dimming and brightening: A review, J. Geophys. Res., 114, D00D16, doi:10.1029/2008JD011470, 2009.

Williams, C. A. and Hanan, N. P.: ENSO and IOD teleconnections for African ecosystems: evidence of destructive interference between climate oscillations, Biogeosciences, 8, 27–40, doi:10.5194/bg-8-27-2011, 2011.

Wolter, K. and Timlin, M. S.: Measuring the strength of ENSO events – how does 1997/98

rank?, Weather, 53, 315–324, 1998.

Wooster, M. J., Perry, G. L. W., and Zoumas, A.: Fire, drought and El Niño relationships on Borneo during the pre-MODIS era (1980–2000), Biogeosciences Discuss., 8, 975–1013, doi:10.5194/bgd-8-975-2011, 2011.

Woodward, F. I., Lomas, M. R., and Quaife, T.: Global responses of terrestrial productivity to contemporary climatic oscillations, Philos. T. Roy. Soc. B, 363, 2779–2785, 2008.

Xiao, J. F., Zhuang, Q. L., Baldocchi, D. D., Law, B. E., Richardson, A. D., Chen, J., Oren, R., Starr, G., Noormets, A., Ma, S., Verma, S. B., Wharton, S., Wofsy, S. C., Bolstad, P. V., Burns, S. P., Cook, D. R., Curtis, P. S., Drake, B. G., Falk, M., Fischer, M. L., Foster, D. R., Gu, L., Hadley, J. L., Hollinger, D. Y., Katul, G. G., Litvak, M., Martin, T., Matamala, R., McNulty, S., Meyers, T. P., Monson, R. K., Munger, J. W., Oechel, W. C., Paw, U., Kyaw, T., Schmid, H. P., Scott, R. L., Sun, G., Suyker, A. E., and Torn, M. S.: Estimation of net ecosystem carbon exchange for the conterminous United States by combining MODIS and AmeriFlux data, Agr. Forest Meteorol., 148, 1827–1847, 2009.

Yang, F., White, M. A., Michaelis, A. R., Ichii, K., Hashimoto, H., Votava, P., Zhu, A.-X., and Nemani, R. R.: Prediction of continental scale evapotranspiration by combining MODIS and AmeriFlux data through Support Vector Machine, IEEE T. Geosci. Remote, 44, 3452–3461, 2006.

Yang, L., Ichii, K., White, M. A., Hashimoto, H., Michaelis, A. R., Votava, P., Zhu, A.-X., Huete, A., Running, S. W., and Nemani, R. R.: Developing a continental-scale measure of gross primary production by combining MODIS and AmeriFlux data through support machine approach, Remote Sens. Environ., 110, 109–122, 2007.

Yeh, S. W., Kug, J. S., Dewitte, B., Kwon, M. H., Kirtman, B. P., and Jin, F. F.: El Niño in a changing climate, Nature, 461, 511–514, doi:10.1038/nature08316, 2009.

Zeng, N., Mariotti, A., and Wetzel, P.: Terrestrial mechanisms of interannual CO_2 variability, Global Biogeochem. Cy., 19, GB1016, doi:10.1029/2004GB002273, 2005.

Table 1. Flux anomaly, uncertainty, intensity, and duration of El Niño events from 1997–2009. Positive anomaly values indicate increased outgassing of CO$_2$ to the atmosphere. Reported uncertainties represent 1σ. Δ_{biotic}: uncertainties in water deficit from MERRA and FLUXNET-derived sensitivity combined using Monte Carlo methods. Δ_{fire}: 20 % annual relative error (van der Werf et al., 2010). Δ_{total}: uncertainties for Δ_{biotic} and Δ_{fire} summed in quadrature. For the Jena inversion (update of Rödenbeck et al., 2003, 2005) uncertainties calculated as mean absolute deviation over a 6-member ensemble. Mean event rows show annualized mean and σ across El Niño events. The Jena inversion record ends in 2008. The 2009 El Niño event continues in 2010 but GFED version 3.1 data extends only through 2009. Overlapping events are those with Δ_{biotic} and Δ_{fire} as well as Jena inversion estimates, i.e., the first four events only.

El Niño Events	Mean MEI Value	Duration (months)	Event Flux Anomaly (Pg C yr^{-1})			
			Δ_{biotic}	Δ_{fire}	Δ_{total}	Jena
April 1997–June 1998	2.16	15	-0.25 ± 0.04	0.53 ± 0.11	0.28 ± 0.11	2.48 ± 0.15
April 2002–April 2003	0.83	13	0.39 ± 0.03	0.10 ± 0.02	0.48 ± 0.04	1.19 ± 0.03
May 2004–May 2005	0.59	13	0.13 ± 0.03	0.05 ± 0.01	0.18 ± 0.04	-0.48 ± 0.07
June 2006–February 2007	0.83	9	-1.34 ± 0.02	0.19 ± 0.04	-1.15 ± 0.05	-1.01 ± 0.02
June 2009–December 2009	0.94	7	0.98 ± 0.03	-0.49 ± 0.10	0.49 ± 0.10	–
Mean (all events)	1.07	11.4	-0.02 ± 0.86	0.08 ± 0.37	0.06 ± 0.69	–
Mean (overlapping events)	1.11	12.5	-0.27 ± 0.76	0.22 ± 0.22	-0.05 ± 0.74	0.55 ± 1.60
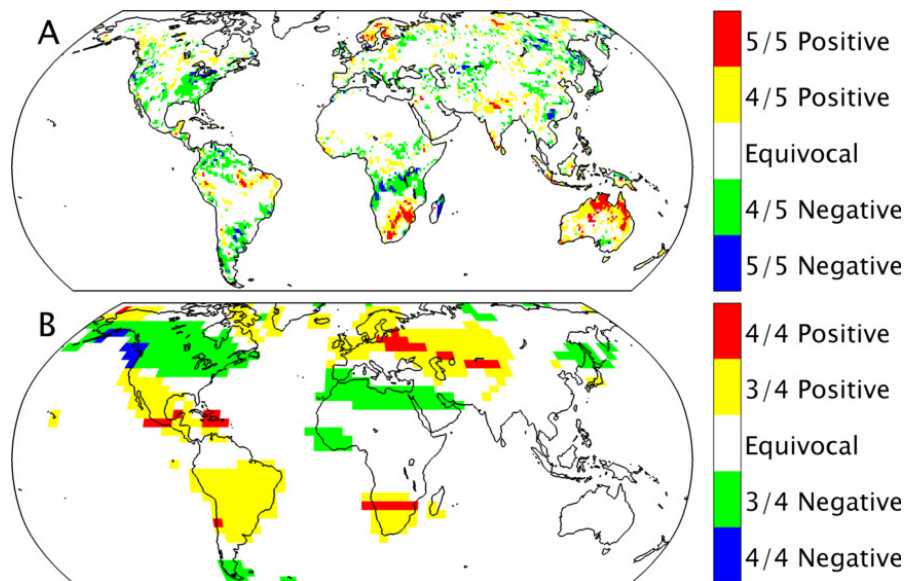
Fig. 1. Terrestrial carbon sink anomaly sign across multiple El Niño events. **(A)** Patterns of Δ_{biotic} sign ($1° \times 1°$) for 5 El Niño events from 1997–2009. **(B)** Patterns of Jena inversion-based sign of NEE anomaly ($3.75° \times 5°$) for 4 El Niño events from 1997–2008. Legend numbers indicate the number of events out of all 5 (4 for **B**) with the relevant sign. Non-vegetated grid cells and those with signs split 2 to 3 (2 to 2 for **B**) shown in white. A positive sign indicates increased outgassing of CO_2 to the atmosphere.
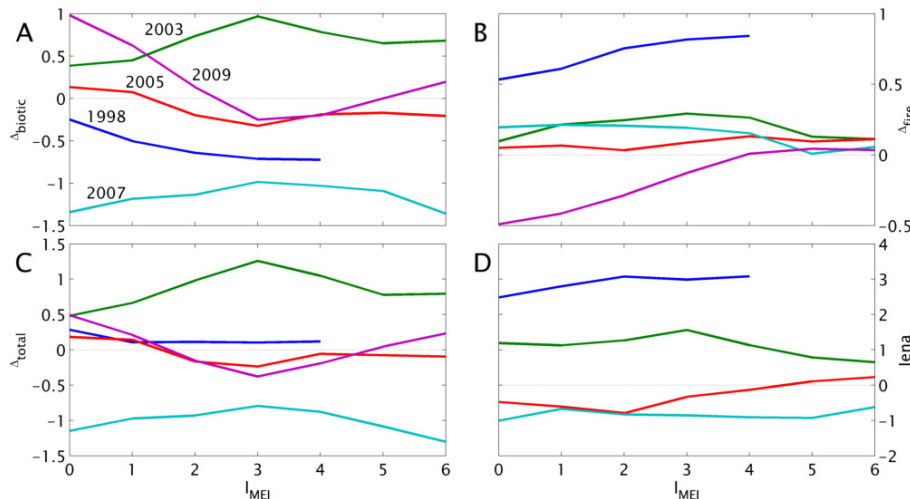
Fig. 2. Global flux anomaly as a function of time-lag for 5 El Niño events from 1997–2009. El Niño events (colored lines) indexed by year **(A)**. Lags (I_{MEI}) from 0 to 6 months shown; flux anomaly always lags MEI. Flux anomalies (Pg C yr^{-1}) are Δ_{biotic} **(A)**, Δ_{fire} **(B)**, Δ_{total} **(C)**, and Jena inversion **(D)**. The 1997/1998 event (blue line) cannot be calculated with a lag of 5 or greater as it began in April and a time delay of 5 or more months was not observed. A positive sign indicates increased outgassing of CO$_2$ to the atmosphere.
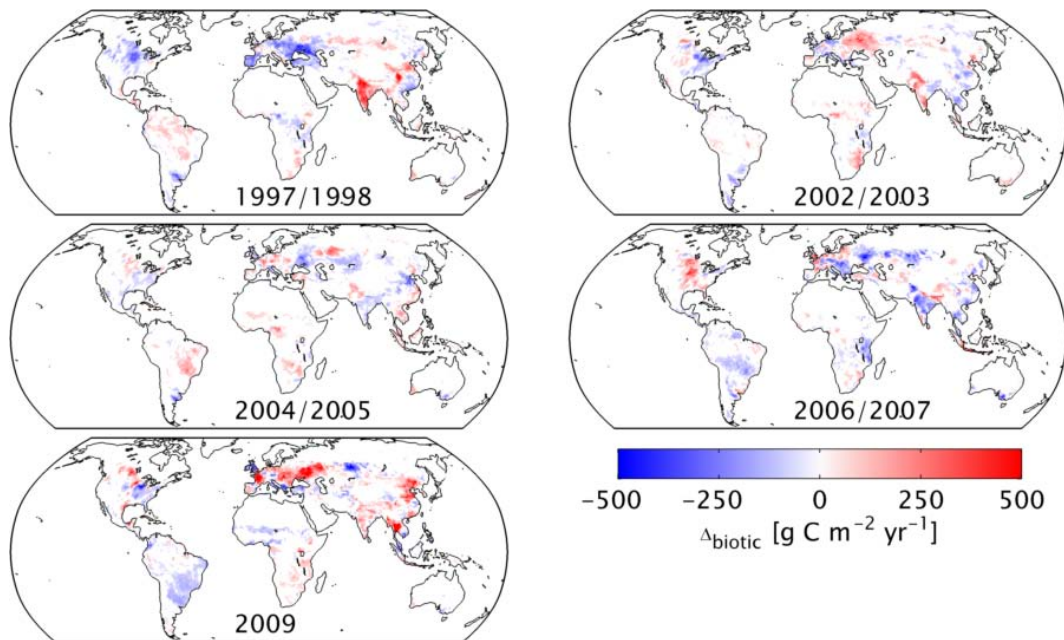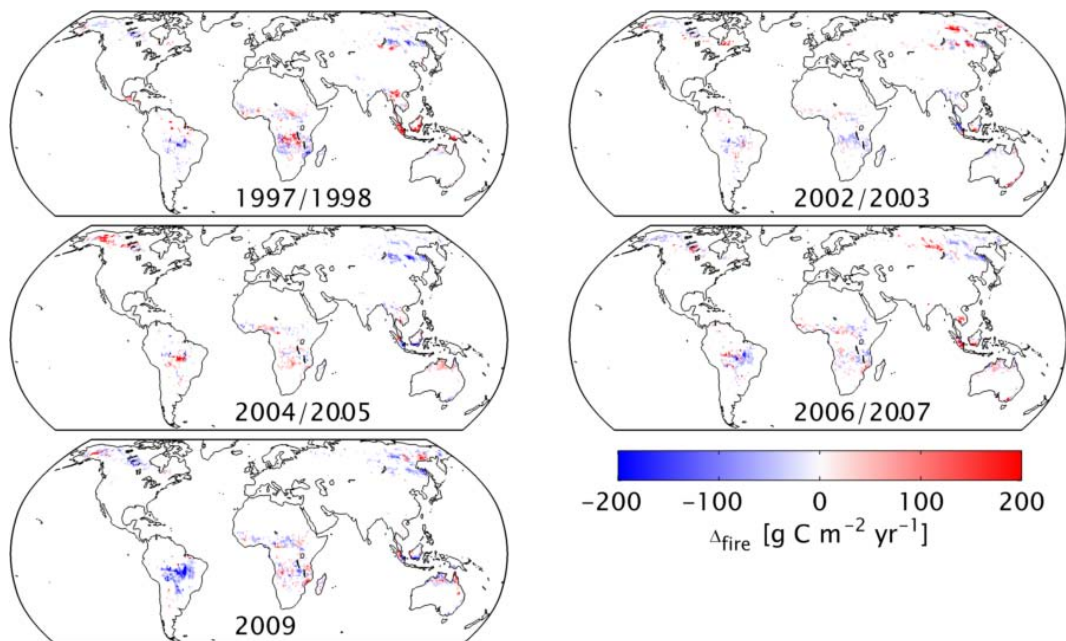
Fig. 3. Patterns of Δ_{biotic} (g C m^{-2} yr^{-1}) for 5 El Niño events from 1997–2009. Inset years denote El Niño event; panel insets show insular Southeast Asia. Values are event totals scaled to 1 yr. Non-vegetated grid cells and $|\Delta_{biotic}| \leq 50$ g C m^{-2} yr^{-1} shown in white. For the 2009 event 61 grid cells in temperate Eurasia and Indochina have values from 500 to 1166 g C m^{-2} yr^{-1}. Positive anomalies indicate increased CO$_2$ outgassing (decrease in sink strength) and vice versa.

Title Page

Abstract | Introduction

Conclusions | References

Tables | Figures

◀◀ | ▶▶

◀ | ▶

Back | Close

Full Screen / Esc

Printer-friendly Version

Interactive Discussion

Fig. 4. Patterns of Δ_{fire} (g C m^{-2} yr^{-1}) for 5 El Niño events from 1997–2009. Inset years denote El Niño event; panel insets show insular Southeast Asia. Values are event totals scaled to 1 yr. Non-vegetated grid cells and $|\Delta_{fire}| \leq 25$ g C m^{-2} yr^{-1} shown in white. Positive anomalies indicate increased fire emissions and vice versa.
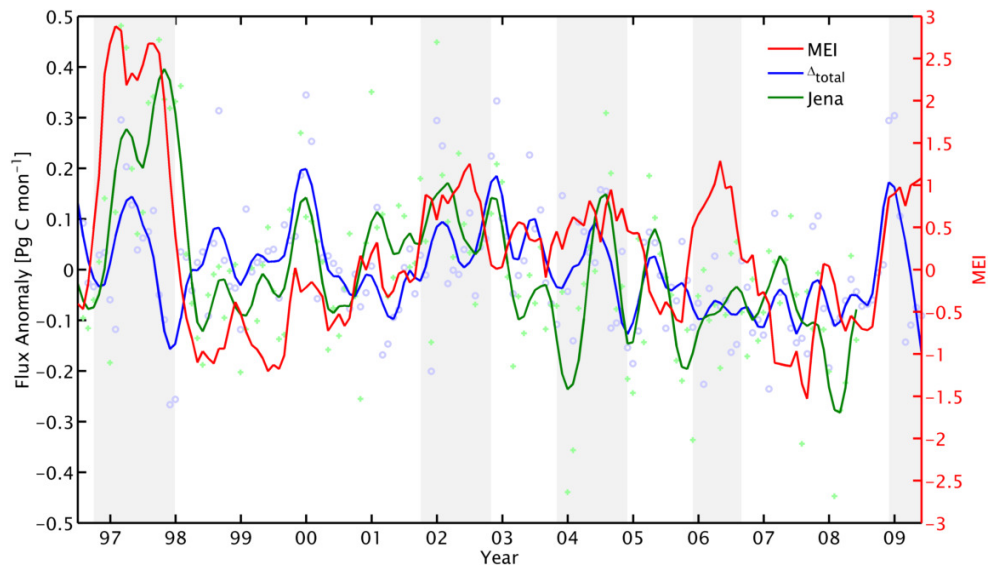
Fig. 5. Temporal profiles of global flux anomaly and MEI from 1997–2009. Monthly time series show MEI (red), Δ_{total} (blue), and Jena (green). For clarity the time series for Δ_{total} and Jena were loess smoothed with a 12-month span. Lighter symbols show unsmoothed anomalies. Year label is centered on June-to-August. Grey background indicates El Niño event. Jena inversion results only available from 1997–2008.
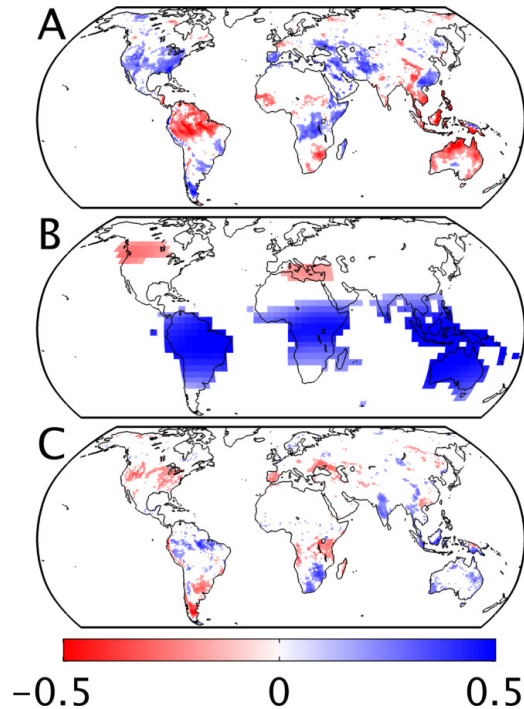
Fig. 6. Teleconnections with MEI. Correlations between MEI and water deficit anomalies **(A)**, MEI and Jena inversion results **(B)**, MEI and Δ_{biotic} **(C)**. Correlations were computed on a monthly time step for each pixel relative to MEI across the full analysis period (1997–2009). Non-vegetated grid cells and pixels without significant teleconnections ($p > 0.05$) shown in white.
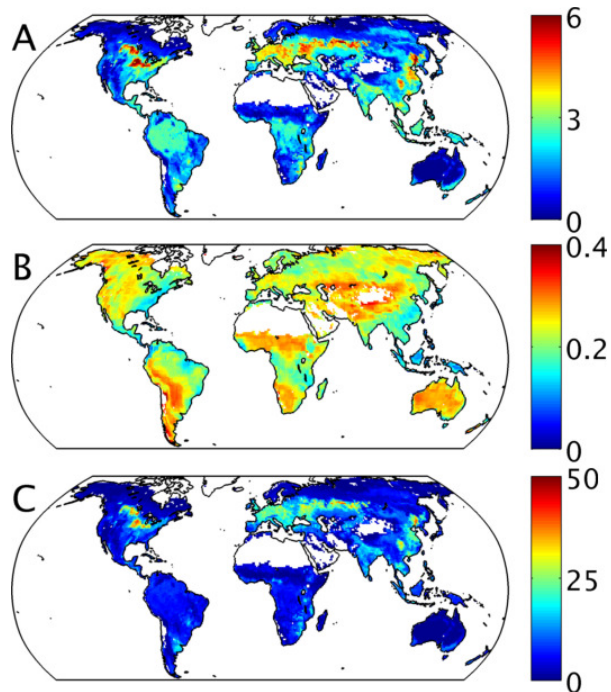
Fig. 7. Component and total uncertainty in biotic flux anomaly. Uncertainties are (1σ) for each grid cell across all months (1997–2009). **(A)**: uncertainty (g C m^{-2} month^{-1}) in NEE sensitivity to water deficit (Schwalm et al., 2010a). **(B)**: uncertainty (dimensionless) in water deficit based on a 10-member ensemble of reanalysis products (Bosilovich et al., 2009). **(C)**: total uncertainty ($\varepsilon_{\text{biotic}}$, g C m^{-2} month^{1}) in Δ_{biotic} from combining component uncertainties (**A** and **B**) using Monte Carlo techniques. Uncertainty was time-averaged with weights from GIMMS f_{PAR} normals (Tucker et al., 2005) to emphasize periods of greater biological activity. Non-vegetated grid cells shown in white. Note different color scales.